UNIVERSITY OF COPENHAGEN
DEPARTMENT OF CHEMISTRY

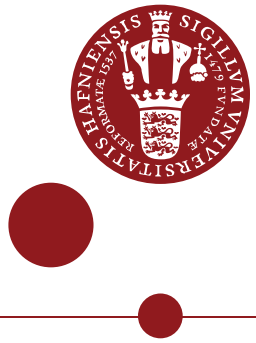

Supplementary Information

Marcus Nørgaard Weng

Machine learning on simulated high entropy alloy catalysis for fuel cells

Supervisor: Jan Rossmeisl

Submitted on: 31 October 2023

Name of department:	Department of Chemistry
Author(s):	Marcus Nørgaard Weng
Title and subtitle:	Machine Learning on simulated high entropy alloy catalysis for fuel cells
Topic description:	The project is about understanding high entropy alloy catalysis in fuel cell reactions. High entropy alloys are an increasingly researched topic partly because of their promising catalytic abilities. Fuel cells is an important use case of new catalysts, since they rely on good catalytic properties to function efficiently. Fuel cells can provide energy without greenhouse gas emissions and has applications where other green energy sources will not suffice and can therefore be a part of the technological solution to the climate crisis. The subject of the project is data treatment of DFT simulations of high entropy alloy catalysts and producing accurate models for fuel cell high entropy alloys during activity. The methods used for producing results will include machine learning and statistics.
Supervisor:	Jan Rossmeisl
Submitted on:	31 October 2023
Number of characters:	12.604

Table of contents

Supplementary Information

Literature DFT calculations on CO-poisoning mechanisms

In an article by Zhong et. al., each structure through the reaction steps and transition state has been simulated with DFT and relaxed, reporting the energies at each step and transition state[1]. Using this technique, transition state structures were suggested, along with a new proposed pathway leading to CO. The new proposed pathway is a reaction between two HCOOH molecules stabilized near the surface by various water molecules and each other, going through a transition state, where one HCOOH loses its OH group, forming a water molecule with the C-bound H from the other HCOOH, and losing its H. This results in a bound CO, while the other HCOOH is oxidated into CO_2. The reaction diagram looks like this:

$$HCOOH + HCOOH \rightarrow CO_2 + 2(H^+ + e^-) + CO^* + H_2O$$

The article calculates the energy barrier of the proposed reaction to 15.1 kCal/mol, which is higher than the energy barrier of the direct pathway, 5.8 kCal/mol, but half the energy barrier of the indirect pathway, 32.1 kCal/mol, indicating that the 2 HCOOH pathway might be a realistic explanation of the CO-poisoning phenomenon. This is different from the setup from the indirect pathway, which requires the adsorbates H and COOH on neighbouring sites, while the 2 HCOOH pathway requires a HCOOH dimer on or around neighbouring site, so even if this pathway is the dominant in the formation of CO, it should be discouraged by single-site catalysts, which would possibly deter neighbouring H+COOH as well as HCOOH+HCOOH stabilized near the surface. Furthermore, the results from Bagger et. al. showed a highly deprecated performance after setting the anode potential vs RHE to near-zero values and returning to previously highly active potentials[2]. Hydrogen under-potential deposition (H_{UPD}) is known to happen at near-zero potentials, which indicates that it plays a role in the decreased activity. The fact that the catalytic activity decreases significantly after visiting potentials where H adsorbs indicates that the cause could be the H and COOH disproportionation reaction. The COOH+COOH reaction might be causing CO poisoning at higher potentials, but not at the same rate as the indirect FAOR pathway, as shown by the cyclic voltammograms in Bagger et. al. This is due to the disproportionation reaction being possible only at low potentials, which is seen to decrease FAOR performance greatly, while COOH+COOH should happen more seldomly at smaller potentials, where fewer sites will bind COOH.

Modelling the activity of a catalytic site

The activity of chemical reactions is limited by the energy of the activated complex, E_a. The energy of the activated complex is related to the binding energy, which we can model. The binding energies and potential are used to predict a relative measure of the current density with the following equations based on the Arrhenius-like equation[3,4]:

$$j_{k,i} = e^{-\frac{\Delta G_{RLS}}{k_B \cdot T}}$$

$$\Delta G_{RLS} = \left|\Delta G_i - \Delta G_{opt}\right| - eU_{opt} + eU$$

Where $j_{k,i}$ represents the per-site current density in arbitrary units, e represents Eulers number, ΔG_{RLS} represents the energy of the rate-limiting step, k_B represents the Boltzmann constant, and T represents the temperature in Kelvin. ΔG_i represents the binding energy at site i and ΔG_{opt} represents the optimal binding energy at site i. U_{opt} represents the optimal potential and U represents the potential. The Gibbs free energy of the rate-limiting step term will be zero, when the binding energy and potential are optimal, leading to the largest possible per-site activity. The denominator $k_B T$ determines the "width" of the Sabatier volcano, dictating how harshly sub-optimal binding energies and potentials are punished in terms of decreased activity. At 300 K, $k_B T$ is 0.02585 eV, meaning even a relatively small difference between the optimal binding energy and the actual binding energy of $0.02585\ eV$ decreases the activity from 1 in the optimal case to 0.367. The Koutecký-Levich equation is used to calculate the current density j_i, accounted for diffusion-limits:

$$\frac{1}{j_i} = \frac{1}{j_D} + \frac{1}{j_{k,i}}$$

Where j_D represents the diffusion-limited current and $j_{k,i}$ represents the kinetically limited current.

$$j = \frac{1}{N}\sum_{i}^{N_{ads}} j_i$$

The average current density over the whole catalyst surface is calculated with the summed current densities divided by the number of sites.

The method described assumes a Sabatier volcano relationship between the adsorption energies. A different relative measure that can be used to compare different simulated catalyst surfaces, that doesn't assume a Sabatier relationship is counting the number of sites where the adsorbate binds at a potential, and assuming that those are equally active.

This measure can be justified for the direct pathway of FAOR, because if the binding energy of formate is negative, but larger than $-\ 0.34\ eV$, using formic acid as a reference, formate binds and the energy necessarily decreases in the final step leading to CO_2, because the energy of the CO_2 decreases with $-2U$, and formate only $-U$. No catalyst in this work has the strength to bind formate stronger than $-0.34\ eV$ at no anode potential, so formate is guaranteed to react, if it has a negative adsorption energy and binds to the catalyst. The sum of the active sites set to have a current density of 1 can then be adjusted for diffusion-limits and averaged, similarly to the previously described current density measure.

GPAW

This work carries out DFT calculations with the Python implementation and package GPAW[5]. The Python package GPAW is built on the Atomic Simulation Environment (ASE)[6].
The GPAW package uses the Projector-Augmented Wave (PAW)-method, which uses pseudo wave-functions to represent inner-core electrons, instead of the more computationally expensive, but more precise "all-electron" method[7,8]. The PAW method relies on a few approximations in order to justify the pseudo wave-functions e.g. the core orbitals are assumed to be "frozen" and a finite number of basis and projector functions are assumed to be sufficient to describe the wave functions. Core electrons are subjected to strong interactions due to the positively charged nucleus, making them highly oscillatory, needing many basis functions to describe[9]. Hence, smooth pseudo wave-functions are used to describe them to lower the computational requirements. The smooth pseudo wave-functions can be described on the form:

$$\tilde{\psi}^a(r) = \sum_i C_i^a \tilde{\phi}_i^a\ (\boldsymbol{r})$$

Where $\tilde{\phi}_i$ are atom-centered basis functions and C_i^a are expansion coefficients given as:

$$C_i^a = \int d\boldsymbol{r} \tilde{p}_i^a(\boldsymbol{r} - \boldsymbol{R}^a)\tilde{\psi}(\boldsymbol{r})$$

With the nuclei and core electrons described by a pseudopotential, the Kohn-Sham equations are only solved for the remaining valence electrons.

Periodic systems

The sites investigated in this work are on flat fcc(111) surfaces, hence the DFT simulated surfaces should reflect this. To achieve an effectively infinite flat fcc(111) metal surface, periodic boundary conditions are implemented in the DFT routine around the 3x3x5 metal HEA slab unit cells. The periodic boundary conditions are effectuated in the x-y plane, resulting in a repeating 3x3 top layer. The effective size of the size will be infinite, but the same atoms will

repeat periodically, making a unit cell, which in turn, requires the wavefunction to be periodic. According to Bloch's theorem solutions to the Schrödinger Equations in a periodic potential can be described as plane waves modulated by periodic functions[10]:

$$\psi(\boldsymbol{r}) = e^{i\boldsymbol{k}\cdot\boldsymbol{r}}u(\boldsymbol{r})$$

Where ψ is the wave function as a function of position r and $u(r)$ is a periodic function with the same periodicity as the unit cell. To keep the number of plane waves feasible for calculation with numeric methods, an energy cut-off is used as a relevance criterion. In GPAW, a maximum kinetic energy (in eV) for the plane-wave electron is set, selecting the plane waves that obey:

$$\frac{|G+k|^2}{2} < E_{cut}$$

GPAW (Grid-based Projector-Augmented Wave) uses a grid-based approach, where the simulation space is divided into a three-dimensional grid of points. The smooth wave-functions are evaluated at each point in grid point in real space. The grid spacing is determined by the parameter h in Å. The quality of the simulation is dependent on the grid-spacing used for the real-space representations of the wave functions, as a smaller grid-spacing results in a better convergence of the total energy[5]. The Brillouin zone is a region defined in reciprocal space, often used in solid-state physics and material chemistry for electronic properties in crystalline materials due to its symmetry properties. Sampling the Brillouin zone means sampling "k-points" in momentum space. In GPAW, the Brillouin zone is sampled with a grid of k-points that is Monkhorst-Pack sampled, which will sample the Brillouin zone with a regular grid of N1xN2xN3 k-points. The k-point density has the expression:

$$N\frac{a}{2\pi}$$

Where N is the number of k-points and a is the length of the unit-cell along the reciprocal lattice vector.

Single-sites in random mixing

Firstly, some notation is established. A surface composition is given as A_aB_b with f(A) = a and f(B) = b indicating the stoichiometry of each metal. The stoichiometries sum to unity. A single-site it defined as a motif where an A metal is surrounded by six B metals on an fcc(111) surface. The atoms are assumed to be distributed randomly on the hexagonal closest packed top layer of the fcc(111) surface. The task at hand is then to find the stoichiometry that will lead to the statistically highest random occurrence of single-sites. The odds of finding an A metal at a specific position is f(A), and the odds of finding a B metal on a neighbouring site is f(B) or 1 –

f(B). The odds of finding six neighbouring B metals independently are then (1 - f(B))^6. The odds of finding a single-site (ss) are then:

$$f(ss) = f(A) * \left(1 - f(A)\right)^6$$

Increasing the contents of A increases the odds of finding A metals that could possibly be a single-site, but at the same decreases the odds of finding six B metals surrounding it. To find the equilibrium f(A) that maximizes f(ss) the function is afledt ift f(A) and set equal to zero, and isolating f(A), finding a top-point

$$\frac{df(ss)}{df(A)} = \left(1 - f(A)\right)^6 - 6 \cdot f(A) \cdot \left(1 - f(A)\right)^5 = 0$$

$$f(A) = \frac{1}{7}$$

The maximum per-atom odds of finding a ss is:

$$f(ss) = \frac{46656}{823543} = 5.66\ \%$$

When including two B metals, that bind H and COOH weakly, they can share the $\frac{6}{7}$ fraction amongst them, eg. $A_{\frac{1}{7}}B1_xB2_{\frac{6}{7}-x}$.

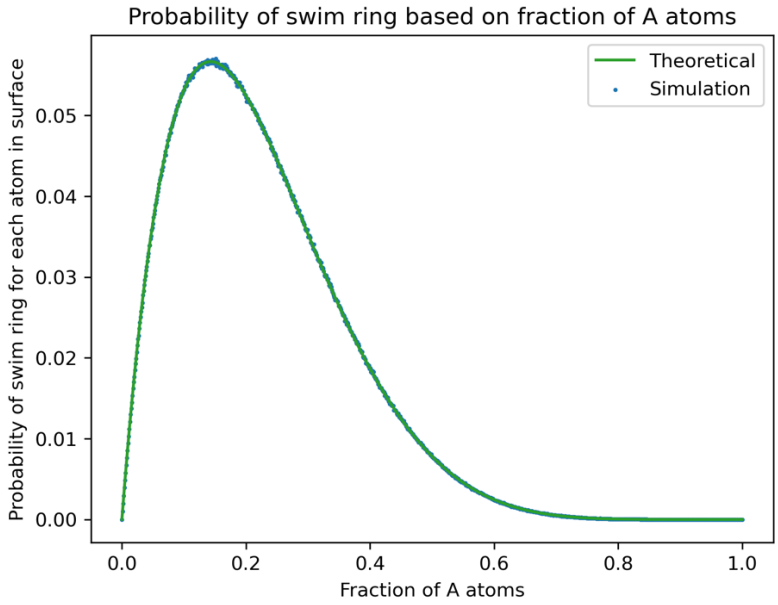

Figure 1 - A comparison between the probability of finding a single-site structure at each on-top site on a randomly mixed fcc(111) surface as a function of the fraction of A atoms, as calculated with the theoretical approach (solid line) and as simulated on 1000 by 1000 surfaces at each fraction of A atoms.

The results have been verified by a simulation, as shown in figure 8. In the simulation, a 1000 by 1000 top layer of a surface have been created with a range of 1000 evenly spaced f(A) values between 0 and 1. The number of ss are found by scanning each site on each surface.

References

(1) Zhong, W.; Zhang, D. New Insight into the CO Formation Mechanism during Formic Acid Oxidation on Pt(111). *Catal. Commun.* **2012**, *29*, 82–86. https://doi.org/10.1016/j.catcom.2012.09.002.

(2) Bagger, A.; Jensen, K. D.; Rashedi, M.; Luo, R.; Du, J.; Zhang, D.; Pereira, I. J.; Escudero-Escribano, M.; Arenz, M.; Rossmeisl, J. Correlations between Experiments and Simulations for Formic Acid Oxidation. *Chem. Sci.* **2022**, *13* (45), 13409–13417. https://doi.org/10.1039/D2SC05160E.

(3) Batchelor, T. A. A.; Pedersen, J. K.; Winther, S. H.; Castelli, I. E.; Jacobsen, K. W.; Rossmeisl, J. High-Entropy Alloys as a Discovery Platform for Electrocatalysis. *Joule* **2019**, *3* (3), 834–845. https://doi.org/10.1016/j.joule.2018.12.015.

(4) Pedersen, J. K.; Clausen, C. M.; Krysiak, O. A.; Xiao, B.; Batchelor, T. A. A.; Löffler, T.; Mints, V. A.; Banko, L.; Arenz, M.; Savan, A.; Schuhmann, W.; Ludwig, A.; Rossmeisl, J. Bayesian Optimization of High-Entropy Alloy Compositions for Electrocatalytic Oxygen Reduction**. *Angew. Chem.* **2021**, *133* (45), 24346–24354. https://doi.org/10.1002/ange.202108116.

(5) Mortensen, J. J.; Hansen, L. B.; Jacobsen, K. W. Real-Space Grid Implementation of the Projector Augmented Wave Method. *Phys. Rev. B* **2005**, *71* (3), 035109. https://doi.org/10.1103/PhysRevB.71.035109.

(6) Hjorth Larsen, A.; Jørgen Mortensen, J.; Blomqvist, J.; Castelli, I. E.; Christensen, R.; Dułak, M.; Friis, J.; Groves, M. N.; Hammer, B.; Hargus, C.; Hermes, E. D.; Jennings, P. C.; Bjerre Jensen, P.; Kermode, J.; Kitchin, J. R.; Leonhard Kolsbjerg, E.; Kubal, J.; Kaasbjerg, K.; Lysgaard, S.; Bergmann Maronsson, J.; Maxson, T.; Olsen, T.; Pastewka, L.; Peterson, A.; Rostgaard, C.; Schiøtz, J.; Schütt, O.; Strange, M.; Thygesen, K. S.; Vegge, T.; Vilhelmsen, L.; Walter, M.; Zeng, Z.; Jacobsen, K. W. The Atomic Simulation Environment—a Python Library for Working with Atoms. *J. Phys. Condens. Matter* **2017**, *29* (27), 273002. https://doi.org/10.1088/1361-648X/aa680e.

(7) Blöchl, P. E. Projector Augmented-Wave Method. *Phys. Rev. B* **1994**, *50* (24), 17953–17979. https://doi.org/10.1103/PhysRevB.50.17953.

(8) Blöchl, P. E.; Först, C. J.; Schimpl, J. Projector Augmented Wave Method:Ab Initio Molecular Dynamics with Full Wave Functions. *Bull. Mater. Sci.* **2003**, *26* (1), 33–41. https://doi.org/10.1007/BF02712785.

(9) Rostgaard, Carsten. "The Projector Augmented-Wave Method." arXiv Preprint arXiv:0910.1921 (2009).

(10) Bloch, F. □ber die Quantenmechanik der Elektronen in Kristallgittern. *Z. F□r Phys.* **1929**, *52* (7–8), 555–600. https://doi.org/10.1007/BF01339455.